ELSEVIER

Remote Sensing of Environment 78 (2001) 299–313

Remote Sensing of Environment

www.elsevier.com/locate/rse

Investigation of product accuracy as a function of input and model uncertainties Case study with SeaWiFS and MODIS LAI/FPAR algorithm

Yujie Wang[a,*], Yuhong Tian[a], Yu Zhang[a], Nazmi El-Saleous[b], Yuri Knyazikhin[a], Eric Vermote[b], Ranga B. Myneni[a]

[a]*Department of Geography, Boston University, 675 Commonwealth Avenue, Boston, MA 02215, USA*
[b]*NASA Goddard Space Flight Center, Code 922, Greenbelt, MD 20771, USA*

Received 28 June 2000; accepted 24 March 2001

Abstract

The derivation of vegetation leaf area index (LAI) and the fraction of photosynthetically active radiation (FPAR) absorbed by vegetation globally from the Sea-Viewing Wide Field-of-view Sensor (SeaWiFS) multispectral surface reflectances using the algorithm developed for the moderate resolution imaging spectroradiometer (MODIS) instrument is discussed here, with special emphasis on the quality of the retrieved fields. Uncertainties in the land surface reflectance and model used in the algorithm determine the quality of the retrieved LAI/FPAR fields. The in-orbit radiances measured by space-borne sensors require corrections for calibration and atmospheric effects, and this introduces uncertainty in the surface reflectance products. The model uncertainty characterizes the accuracy of a vegetation radiation interaction model to approximate the observed variability in surface reflectances. When the amount of spectral information input to the retrieval technique is increased, not only does this increase the overall information content but also decreases the summary accuracy in the data. The former enhances quality of the retrievals, while the latter suppresses it. The quality of the retrievals can be influenced by the use of uncertainty information in the retrieval technique. We introduce a stabilized uncertainty, which is basic information to the retrieval technique required to establish its convergence; that is, the more the measured information and the more accurate this information is, the more reliable and accurate the algorithm output will be. The quality of retrieval is a function of the stabilized uncertainty whose accurate specification is critical for deriving biophysical surface parameters of the highest quality possible using multispectral land surface data. The global LAI and FPAR maps derived from SeaWiFS multispectral surface reflectances and uncertainty information, as well as an analysis of these products is presented here.

1. Introduction

Leaf area index (LAI) and the fraction of photosynthetically active radiation absorbed by vegetation (FPAR), which characterize vegetation canopy functioning and its energy absorption capacity, are important variables in terrestrial modeling studies of canopy photosynthesis and transpiration. Terrestrial carbon exchange studies with the retrieved structural information show that canopy and landscape structure plays a major role in determining CO_2 fluxes in spatially heterogeneous environments (Sellers et al., 1997). Therefore, these variables are key state parameters in most ecosystem productivity models and in global models of climate, hydrology, biogeochemistry, and ecology (Sellers et al., 1996). Advances in remote sensing technology (Deschamps et al., 1994; Diner et al., 1999; Justice, Vermote, Townshed, et al. 1998) and radiative transfer modeling (Kimes, Knyazikhin, Privette, Abuelgasim, & Gao, 2000; Kuusk, 1985; Myneni, 1991; Ross, Knyazikhin, Kuusk, Marshak, & Nilson, 1992; Ross & Marshak, 1984; Verstraete, Pinty, & Dickenson, 1990) greatly improved the possibility of accurate estimates of biophysical information from spatial, spectral, angular, and temporal resolution of remotely sensing data. The objective of this paper is to demonstrate that uncertainties in multispectral surface reflectances are critical input information to retrieval algorithms in order to derive biophysical surface parameters of the highest quality possible using multispectral land surface data. The operational algorithm for the production of global

* Corresponding author. Tel.: +1-617-353-8342; fax: +1-617-353-8399.
E-mail address: yjwang@bu.edu (Y. Wang).

0034-4257/01/$ – see front matter
PII: S0034-4257(01)00225-5

LAI and FPAR fields developed for the moderate resolution imaging spectroradiometer (MODIS) instrument applied to the Sea-Viewing Wide Field-of-view Sensor (SeaWiFS) data is used to demonstrate this.

At least two factors influence the quality of surface biophysical parameters retrieved from remotely sensed surface reflectances:

• Uncertainty in the land surface reflectance product. Satellite-borne sensors measure in-orbit radiances of the target through the atmosphere. The surface reflectances are obtained by processing the in-orbit data to correct for atmospheric and other environmental effects which lead to uncertainties in the surface reflectance product.

• Model uncertainty determined by the range of natural variation in biophysical parameters not accounted by the model. In general, this type of uncertainty depends on the amount of information available when retrieving biophysical parameters from surface reflectances, as well as the temporal and spatial resolution of data (Diner et al., 1999).

In general, these uncertainties set a limit to the quality of retrievals; that is, accuracy in the retrievals cannot be better than summary accuracy in the data and the model. However, the quality of the retrievals can be influenced by the use of uncertainty information in the retrieval technique. Definitions of uncertainties in the land surface reflectance product and model, as well as their impact on the retrievals, are discussed in Section 3 following a formulation of the inverse problem of retrieving LAI and FPAR from surface spectral reflectances. It is shown that if uncertainties are ignored, it can result not only in the loss of information conveyed by the multispectral data, but also in destabilization of the retrieval process. Results from this section underlie our strategy of producing global SeaWiFS LAI/FPAR fields of highest possible quality.

2. Formulation of the inverse problem

One of the algorithms to retrieve LAI and FPAR from atmospherically corrected Bidirectional Reflectance Distribution Function (BRDF) is formulated as follows (Knyazikhin, Martonchik, Myneni, Diner, & Runing, 1998): Given sun (Ω_0) and view (Ω_v) directions, BRDFs $d_k(\Omega_0,\Omega_v)$ at N spectral bands and uncertainties $\delta_k(\Omega_0,\Omega_v)$ ($k=1, 2, \ldots, N$), find LAI and FPAR. The algorithm compares observed $d_k(\Omega_0,\Omega_v)$ and modeled $r_k(\Omega_0,\Omega_v,p)$ canopy reflectances for a suite of canopy structures and soil patterns that represent a range of expected natural conditions. Here p=[canopy, soil pattern] denotes a pattern of canopy structure and soil type (Kimes et al., 2000). All canopy/soil patterns p for which modeled and observed BRDFs differ by an amount equivalent to or less than the corresponding uncertainty, i.e.

$$\frac{1}{N}\sum_{k=1}^{N}\left(\frac{r_k(\Omega_v,\Omega_0,p)-d_k(\Omega_v,\Omega_0)}{\delta_k}\right)^2 \le 1, \qquad (1)$$

are considered as acceptable solutions. FPAR is also calculated for each acceptable solution. The mean values of LAI and FPAR averaged over all acceptable solutions and their dispersions are taken as solutions and retrieval uncertainties (Kimes et al., 2000; Knyazikhin, Mortonchik, Diner, et al., 1998; Tian et al., 2000; Zhang et al., 2000). If the inverse problem has a unique solution for a given set of surface reflectances, mean LAI coincides with this solution and its dispersion equals zero. If Eq. (1) allows for multiple solutions, the algorithm provides a weighted mean in

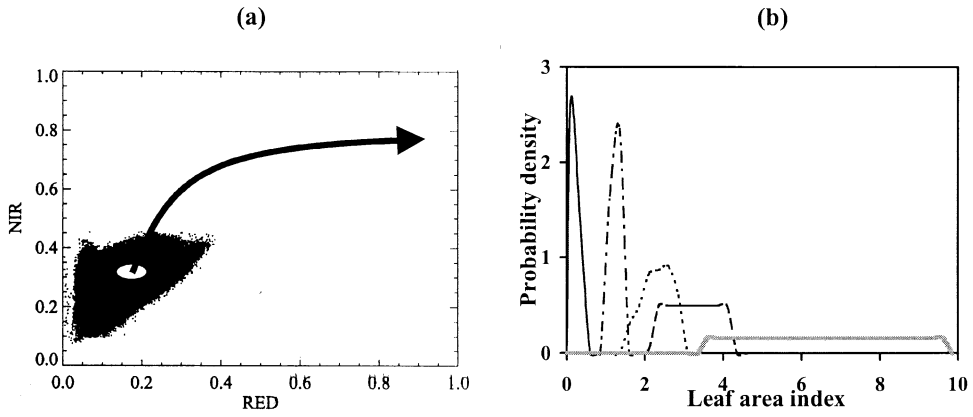

Fig. 1. (a) Distribution of processed pixels with respect to their reflectances at red (d_{RED}) and near-infrared (d_{NIR}) spectral bands derived from SeaWiFS data (September 22, 1997). Inequality (1), $N=2$, defines an ellipse with the semiaxes $\sqrt{2}\delta_{RED}$ and $\sqrt{2}\delta_{NIR}$ centered at the point (d_{RED}, d_{NIR}). Each canopy/soil pattern for which modeled reflectances belong to the ellipse is an acceptable solution. For each set $\mathbf{d}=(d_{RED}, d_{NIR})$ of observed spectral reflectances, one sorts the set of acceptable solutions into ascending order with respect to LAI values and defines a solution distribution function $\Phi_\delta(l,\mathbf{d})$ as the portion of different LAI values, which are less than l. (b) Solution density distribution function $d\Phi_\delta(l,\mathbf{d})/dl$ for five different pixels. Mean LAI over this distribution and its dispersion are taken as LAI retrieval and its uncertainty, respectively.

accordance with the frequency of occurrence of a given value of LAI. The dispersion magnitude indicates the reliability of the corresponding LAI value. The accuracy of retrievals cannot be improved if no additional information is available. Fig. 1 illustrates this approach. Note that the concept of multiple acceptable solutions was originally formulated and implemented in the Multiangle Imaging SpectroRadiometer (MISR) aerosol retrieval algorithm (Martonchick et al., 1998).

In the case of a dense canopy, its reflectance in one or several directions can be insensitive to various parameter values (e.g., LAI) characterizing the canopy because, for example, the reflectance of solar radiation from the underlying soil surface or lower leaf-stories is completely obscured by the upper leaves (Carlson & Ripley, 1997; Jasinski, 1996; Liu & Huete, 1995; Price,1993). When this happens, the canopy reflectance is said to belong to the saturation domain (Knyazikhin, Martonchik, Diner, et al., 1998). The distribution of acceptable LAI values will appear flat over the range of LAI, illustrating that the solutions all have equal probability of occurrence (Fig. 1b). The reliability of LAI values retrieved under a condition of saturation is very low (Gobron, Pinty, & Veratraete, 1997). This situation can be recognized by the retrieval technique (Knyazikhin, Martonchik, Diner, et al., 1998). We introduce a saturation index (SI) as:

$$\mathrm{SI} = \frac{\text{number of LAIs retrieved under conditions of saturation}}{\text{total number of retrieved LAI values}}.$$

This index is an indicator of the quality of the retrievals; that is, the smaller its value, the more reliable the algorithm output would be. One may expect low values of the SI when more information is used to retrieve LAI and FPAR (Diner et al., 1999). However, the SI may increase with increase of uncertainties δ_k.

Given the set $\mathbf{d}=(d_1, d_2, \ldots, d_N)$ of observed canopy reflectances, it may be the case that Eq. (1) has no solutions. A pixel for which the algorithm retrieves a value of LAI and FPAR is termed a retrieved pixel. The ratio of the number of retrieved pixels to the total number of processed pixels is the retrieval index (RI), i.e.:

$$\mathrm{RI} = \frac{\text{number of retrieved pixels}}{\text{total number of processed pixels}}.$$

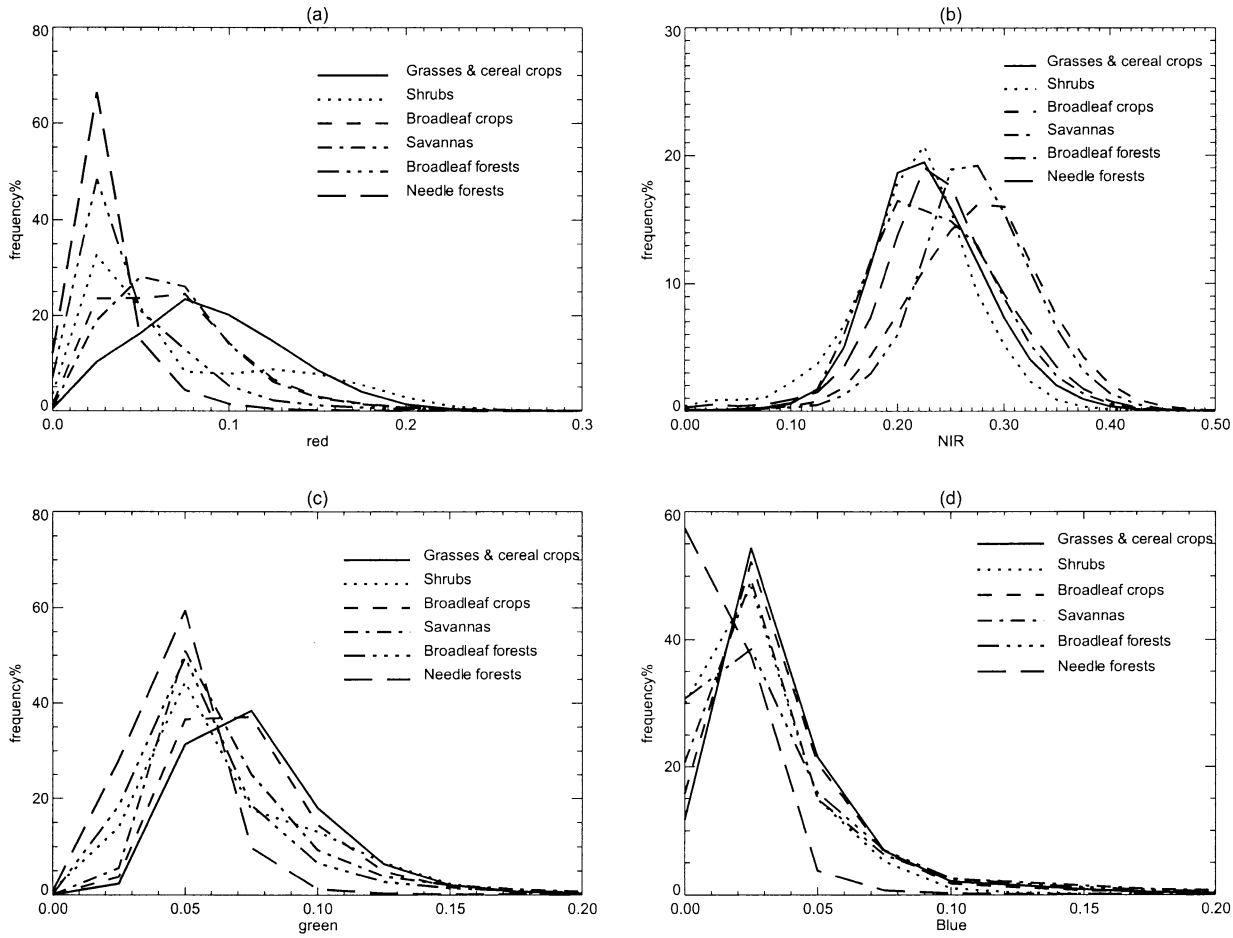

Fig. 2. Histograms of SeaWiFS canopy reflectances in July 1998: (a) red spectral band; (b) near-infrared spectral band; (c) green spectral band; and (d) blue spectral band.

This variable characterizes the quality of LAI and FPAR maps showing of how the retrieved LAI and FPAR values cover the globe. It is a function of uncertainties in the observed and modeled canopy reflectances and number N of spectral bands used. Generally, the RI increases with increasing uncertainties in data and model. However, increasing uncertainties means poor quality of input data and therefore poor quality in LAI/FPAR. Uncertainties, therefore, must be carefully evaluated in order to achieve optimal algorithm performance. A better result should, in general, have a high RI, low SI, and retrieval dispersion.

3. Uncertainties in modeled and observed canopy reflectances

Uncertainties in the land surface reflectance product and model uncertainties set a limit to the quality of retrievals and, thus, their specification is critical to production of global LAI and FPAR of maximum possible quality. Their definitions are presented in this section.

3.1. Uncertainties in the land surface reflectance product

Satellite-borne sensor measures in-orbit radiances of the target through the atmosphere. Obtaining surface reflectances requires processing of the in-orbit data to correct for atmospheric and other environmental effects, which determines uncertainties in the surface reflectance product. Let $d_1, d_2, \ldots, d_N$ be atmospherically corrected BRDFs at N spectral bands. We treat these values as independent random variables with finite variances σ_k^2, $k=1, 2, \ldots, N$, and assume that the deviations $\varepsilon_k=(d_k-m_k)/\sigma_k$ follow Gaussian distribution. Here, m_k is the mathematical expectation of d_k, which are treated as "true values." The random variable

$$\chi_\sigma^2[\mathrm{d}-\mathrm{m}]=\sum_{k=1}^{N}\varepsilon_k^2=\sum_{k=1}^{N}\frac{(d_k-m_k)^2}{\sigma_k^2}, \tag{2}$$

characterizing the proximity of atmospherically corrected data $\mathbf{d}=(d_1, d_2, \ldots, d_N)$ to true values $\mathbf{m}=(m_1, m_2, \ldots, m_N)$ has a chi-square distribution. A value of ${\chi_\sigma}^2 \le N$ indicates good accuracy in the atmospherically corrected surface reflectances. We assume that the atmospheric correction algorithm provides surface reflectances $\mathbf{d}$ satisfying ${\chi_\sigma}^2 \le N$ with a probability $1-\alpha$; that is, $\mathrm{Prob}({\chi_\sigma}^2 > N)=\alpha$ where $1-\alpha$ is the value of the chi-square distribution at N. Dispersions $\sigma=(\sigma_1, \sigma_2, \ldots, \sigma_N)$ are uncertainties in the land surface reflectance product.

3.2. Model uncertainty

Model uncertainty characterizes the accuracy of models to approximate natural variability, which in general is quite high. For example, consider two broadleaf forests (having the same canopy/soil patterns) located, say, in Siberia and in North America. The algorithm treats these as identical scenes. However, their reflectances can differ by 15–20% due to factors that were not accounted in the model. It means that one must assume 15–20% uncertainties in the simulation to account for the fact that these two forests are treated as belonging to one class. This type of uncertainties depend on the amount of information available when retrieving biophysical parameters from surface reflectances, as well as on the temporal and spatial resolution of data.

The propagation of model uncertainty through the retrieval technique starts when one replaces "true" reflectances $\mathbf{m}$ in Eq. (2) with modeled reflectances $\boldsymbol{r}=(r_1, r_2, \ldots, r_N)$. We use values $\varepsilon_{M,k}=(m_k-r_k)/\sigma_{M,k}$, to characterize the inaccuracy in model predictions. Dispersions $\sigma_M=(\sigma_{M,1}, \sigma_{M,2}, \ldots, \sigma_{M,N})$ are model uncertainties. Consider a canopy radiation model that can simulate surface reflectances $\mathbf{m}$ with accuracy $\chi_{\sigma_M}^2[\mathbf{m}-\boldsymbol{r}] \le \boldsymbol{N}$. Based on the Minkowski inequality (Bronstein & Semendyayev, 1985), the following transformation of $\chi_\sigma[\mathbf{d}-\boldsymbol{r}]$ can be performed,

$$\begin{aligned}\chi_\sigma[\mathbf{d}-\mathbf{r}] &= \chi_\sigma[(\mathbf{d}-\mathbf{m})-(\mathbf{r}-\mathbf{m})]\\ &\ge |\chi_\sigma[\mathbf{d}-\mathbf{m}]-\chi_\sigma[\mathbf{m}-\mathbf{r}]|\\ &= \left|\chi_\sigma[\mathbf{d}-\mathbf{m}]-\sqrt{\sum_{k=1}^{N}\frac{(m_k-r_k)^2}{\sigma_k^2}}\right|\\ &= \left|\chi_\sigma[\mathbf{d}-\mathbf{m}]-\sqrt{\sum_{k=1}^{N}\varepsilon_{M,k}^2\frac{\sigma_{M,k}^2}{\sigma_k^2}}\right|.\end{aligned}$$

Thus, $\chi_\sigma[\mathbf{d}-\boldsymbol{r}]$ is a function of the ratio $\sigma_{M,k}/\sigma_k$. Let σ_k tend to zero (i.e., one has very accurate surface

Table 1
Mean reflectance of various biome types

	Biome					
Spectral band	Grass/cereal crops	Shrubs	Broadleaf crops	Savannas	Broadleaf forests	Needle forests
Red	0.104	0.087	0.081	0.083	0.058	0.042
NIR	0.244	0.227	0.288	0.245	0.286	0.255
Blue	0.049	0.038	0.048	0.050	0.047	0.027
Green	0.090	0.078	0.086	0.082	0.073	0.059
NDVI	0.409	0.477	0.559	0.503	0.670	0.713

reflectance measurements) while holding $\sigma_{M,k}$ constant (i.e., the model is not improved). The quantity $\chi_\sigma[\mathbf{d}-\boldsymbol{m}]$ is a bounded value, i.e., $\chi_\sigma[\mathbf{d}-\boldsymbol{m}] \le \sqrt{N}$, while $\chi_\sigma[\mathbf{m}-\boldsymbol{r}]$ becomes arbitrary large. It means that the more accurately atmospheric correction is performed, the more inaccurately the solutions of Eq. (1) approximate LAI values in this case, because the "true" LAI values do not provide a good fit between observed and modeled reflectances. Ignoring the model uncertainty in the retrieval algorithm, therefore, causes a destabilization of the convergence process; that is, the more accurate the input information is, the more reliable the algorithm output should be. This instability also takes place when one uses the metric χ_{σ_M} characterizing the accuracy in model predictions without accounting for the uncertainties in measurements.

To stabilize the convergence process, a stabilized uncertainty $\delta=(\delta_1, \delta_2, \ldots, \delta_N)$ is introduced as $\delta_k^2=(\sigma_{M,k}^2+\sigma_k^2)/\theta^2$. Here, θ is a stabilization parameter as specified below. This uncertainty is used to solve Eq. (1). It follows from the Minkowski inequality that:

$$\begin{aligned}\chi_\delta[\mathbf{d}-\mathbf{r}] &= \chi_\delta[(\mathbf{d}-\mathbf{m})+(\mathbf{m}-\mathbf{r})] \\ &\le \chi_\delta[\mathbf{d}-\mathbf{m}]+\chi_\delta[\mathbf{m}-\mathbf{r}] \\ &= \sqrt{\sum_{k=1}^{N}\frac{(d_k-m_k)^2}{\sigma_k^2}\theta^2\frac{\sigma_k^2}{\sigma_k^2+\sigma_{M,k}^2}} \\ &\quad+\sqrt{\sum_{k=1}^{N}\frac{(m_k-r_k)^2}{\sigma_{M,k}^2}\theta^2\left(1-\frac{\sigma_k^2}{\sigma_k^2+\sigma_{M,k}^2}\right)} \\ &\le \theta\lambda_{\max}\chi_\sigma[\mathbf{d}-\mathbf{m}]+\theta(1-\lambda_{\min})\chi_{\sigma_M}[\mathbf{m}-\mathbf{r}] \\ &\le [\theta\lambda_{\max}+\theta(1-\lambda_{\min})]\sqrt{N}, \end{aligned} \tag{3}$$

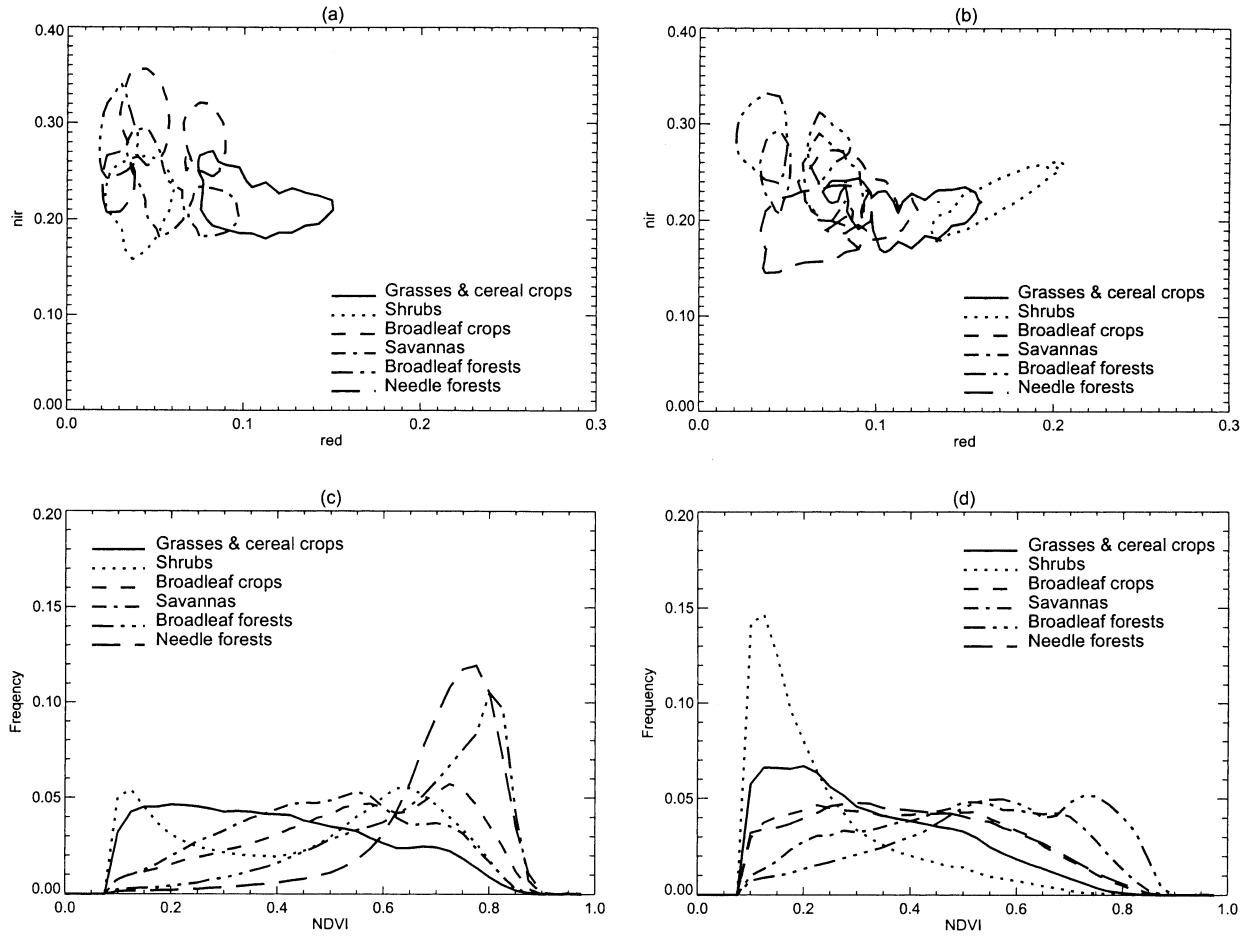

Fig. 3. Statistical properties of SeaWiFS canopy reflectances. Distribution of pixels with respect to their reflectances at red and near-infrared spectral bands in (a) July 1998 and (b) November 1997. Each biome-dependent contour identifies an area of high data density that contains 25% of the pixels from a given biome type. NDVI histograms for six biome types in (c) July 1998 and (d) November 1997.

where:

$$\lambda^2_{\max} = \max_k \frac{\sigma_k^2}{\sigma_k^2 + \sigma_{M,k}^2},$$

$$\lambda^2_{\min} = \min_k \frac{\sigma_k^2}{\sigma_k^2 + \sigma_{M,k}^2}.$$

We assign a value to θ such that $\theta\lambda_{\max} + \theta(1 - \lambda_{\min}) = 1$ is satisfied, i.e., $\theta = 1/(1 + \lambda_{\max} - \lambda_{\min})$. The stabilization parameter varies between 0.5 and 1. It follows from Eq. (3) that the use of the stabilized uncertainty establishes convergence of the retrieval technique; that is, tending σ_k and $\sigma_{M,k}$ to zero independently, "true" LAI always provides a good fit between observed and modeled reflectances within the stabilized uncertainty δ and, thus, solutions of Eq. (1) can approximate the desired parameters.

The metric χ_δ is a decreasing function with respect to the stabilized uncertainty δ. If model and land surface product uncertainties are underestimated (i.e., $\delta < \delta_0$), the algorithm will not admit those solutions of Eq. (1), which provide a good fit in the correct metric χ_{δ_0} and fail in the metric χ_δ. It can result in fewer solutions or even the absence of a solution to Eq. (1) and, consequently, in lower values of the dispersion and RI. For example, all canopy/soil patterns with $\chi_{\delta_0}[\mathbf{d} - \boldsymbol{r}] = \sqrt{N}$, will be treated as unacceptable solutions in this case. The theory of ill-posed problems states that a best estimate of desired parameters satisfies $\chi_{\delta_0}[\mathbf{d} - \boldsymbol{r}] = \sqrt{N}$ (Tikhonov & Arsenin, 1986). Therefore, we cannot expect the decrease in the number of acceptable solutions, the dispersion and the RI to indicate improvement in the algorithm output. On the contrary, the underestimation of real uncertainties can result in the deterioration of retrieval quality.

If model and land surface reflectance uncertainties are overestimated (i.e., $\delta > \delta_0$), then, $\chi_\delta[\mathbf{d} - \boldsymbol{r}] \le \chi_{\delta_0}[\mathbf{d} - \boldsymbol{r}] \le \sqrt{N}$, i.e., the number of solutions to Eq. (1) and, consequently, the RI will increase. It results in a larger number of acceptable solutions, higher RI, and, consequently, lower quality of LAI retrievals. Unlike the former case, however, the best estimation of the desired parameters satisfies Eq. (1). It means that the underestimation of uncertainties can result in a lower retrieval quality than their overestimation. A technique for modification of the algorithm for deriving biophysical parameters of the highest possible quality is equivalent to maximization of RI, minimization of SI and

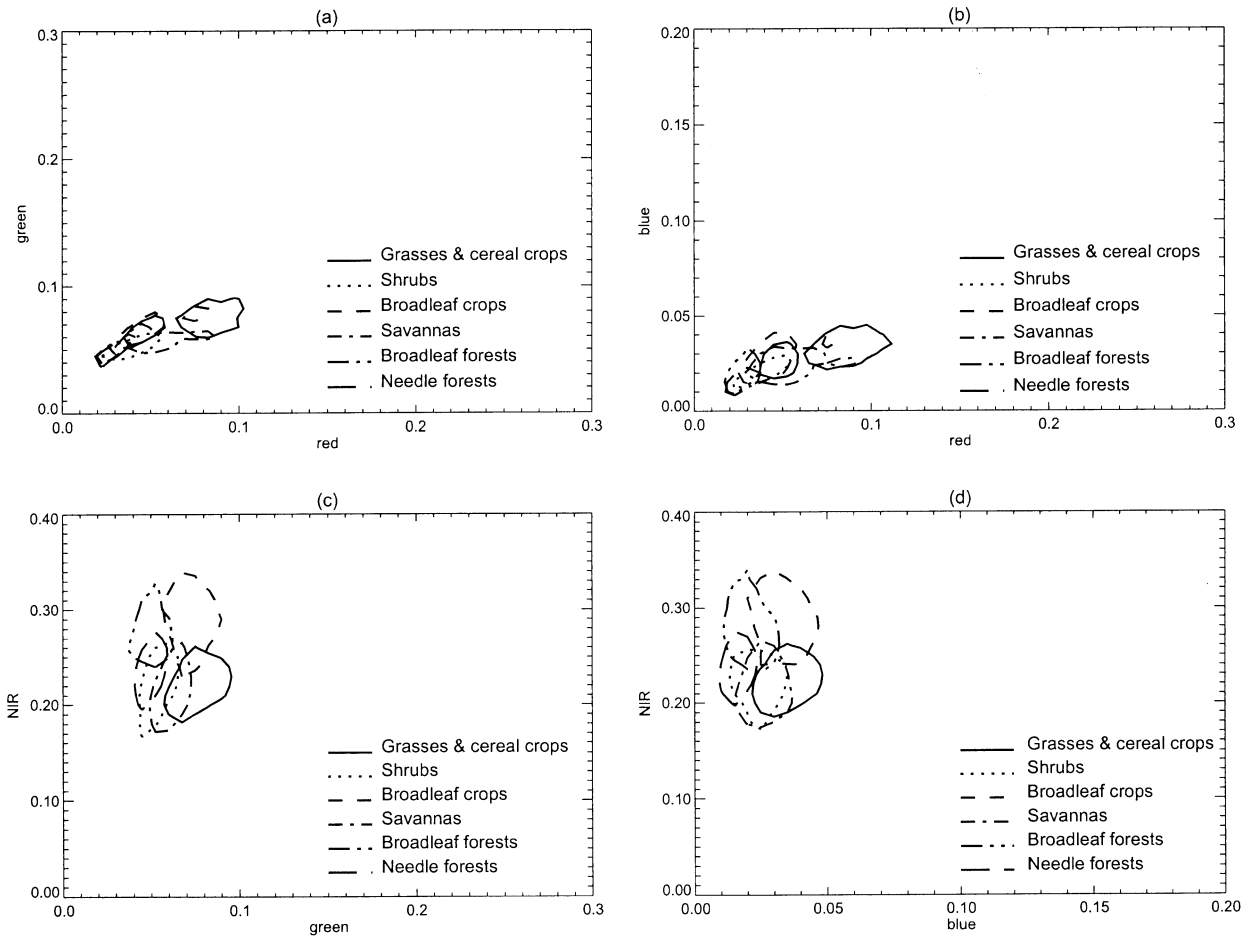

Fig. 4. Twenty-five percent density contours in (a) red–green, (b) red–blue, (c) green–NIR, and (d) in blue–NIR spectral spaces.

Table 2
Theoretical estimation of relative uncertainties in atmospherically corrected surface reflectances (Vermote, 2000)

Spectral band	1 (Red)	2 (NIR)	3 (Blue)	4 (Green)
Center of band, nm	670	865	443	555
Bandwidth, nm	20	40	20	20
Relative error, %	10–33	3–6	50–80	5–12
υ_k, dimensionless	0.2	0.05	0.8	0.1

the dispersion while holding the best estimation in the set of acceptable solutions. Accurate specification of uncertainties should provide a high value of RI for any combination of spectral bands used in Eq. (1). Under this condition, the dispersion, RI, and SI can characterize quality of retrievals.

To study the effect of uncertainties on retrievals, an overall uncertainty $\bar{\delta}$ is introduced as:

$$\bar{\delta} = \sqrt[N]{\delta_1 \delta_2 \cdots \delta_N}$$

where δ_k is the stabilized uncertainty in the ith spectral band. The value of $\sqrt{N}\delta^N$ is proportional to the area (N=2) or volume (N>2) of the ellipse/ellipsoid determined by the inequality (1) in the N-dimensional spectral space (Fig. 1a). In this paper, we will use a relative υ_k and an overall relative $\bar{\upsilon}(N)$ uncertainty defined as:

$$\upsilon_k = \frac{\delta_k}{r_k}, \quad k = 1,\ 2,\ \ldots\ N,$$

$$\bar{\upsilon}(N) = \sqrt[N]{\upsilon_1 \upsilon_2 \cdots \upsilon_N} \tag{4}$$

The overall uncertainty can be considered as a measure of the uncertainty in model and land surface reflectance product. We cannot expect a lower uncertainty in the LAI/FPAR retrievals than the overall uncertainty. Two retrievals are said to be comparable if they were obtained from data having the same value of the overall uncertainty. On this equal-overall uncertainty basis, one can compare different retrievals as a function of the number N of spectral bands used to solve Eq. (1) and uncertainties υ_k, k=1, 2, …, N.

4. Data analysis

Multispectral data from the SeaWiFS were used to produce LAI/FPAR of the highest possible quality with the MODIS algorithm. Geocoded, calibrated, cloud-screened, and atmospherically corrected global surface reflectances in eight spectral bands at 8-km resolution were used in this study. The temporal range of data is September 1997, with nominal mission duration of 5 years. We used surface reflectances centered at 443 (blue), 555 (green), 670 (red), and 865 (near-infrared) nm to retrieve LAI and FPAR with MODIS algorithm (Knyazikhin, Martonchik, Myneni, et al., 1998). The width of the blue, green, and red bands was 20 nm, and NIR was 40 nm. For each pixel, solar and view zenith angles and azimuths were available and are required by the algorithm. The daily data of each month were composited into one layer based on the minimum-blue standard.

A biome classification map (BCM) is another important ancillary data layer used as input to the algorithm. The BCM is derived from the AVHRR Pathfinder data set (Myneni, Nemani, & Running, 1997). In this map, global vegetation is classified into six biome types: grasses and cereal crops; shrubs; broadleaf crops; savannas; broadleaf forests; and needle forests. The structural attributes of these biomes are parameterized in terms of variables that the radiative transfer model admits (Myneni et al., 1997). The three-dimensional transport equation was used to simulate canopy reflectances r_k, k=1, 2, …, N, using the BCM, sun-view geometry and canopy/soil pattern as input (Knyazikhin, Martonchik, Myneni, et al., 1998).

4.1. Spectral signature of the SeaWIFs surface reflectances

Fig. 2 presents histograms of canopy reflectances for different spectral bands and biome types and Table 1 shows mean values of these histograms. Typically, global canopy reflectance varies between 0 and 0.2 at the red band, 0.1 and 0.4 at the NIR band, 0 and 0.15 at the green band, and less than 0.1 at the blue band. On the average, needle forests have the strongest absorption in red, green, and blue bands, but have a stronger reflectance in the NIR band. Grasses can be regarded as the "brightest" biome exhibiting almost the highest reflectances in red, green, and blue bands. Broadleaf crops have a strong reflectance in both NIR and red bands while the reflectance of broadleaf forests is strong in NIR but very low in the red band.

The Normalized Difference Vegetation Index (NDVI) is defined as $(d_{\mathrm{NIR}} - d_{\mathrm{R}})/(d_{\mathrm{NIR}} + d_{\mathrm{R}})$, where d_{NIR} and d_{R} are observed reflectances at the NIR and red band, respectively. The NDVI is a very important measure of chlor-

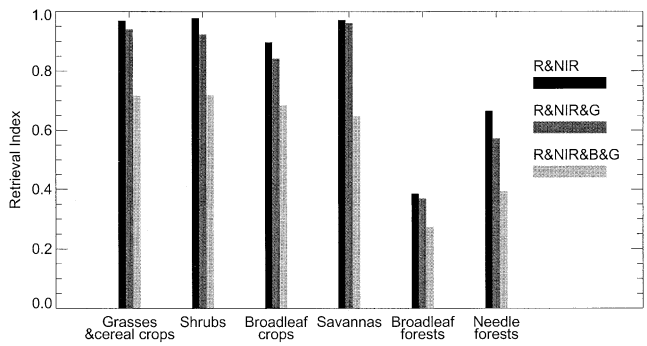

Fig. 5. RI for various biome types and spectral bands used to produce LAIs. R&NIR: red and near-infrared bands; R&NIR&G: red, near-infrared, and green bands; R&NIR&B&G: red, near-infrared, blue, and green bands. Relative uncertainties were set to the upper bound 0.2.

Table 3
RI for various combinations of spectral bands used to retrieve LAI and FPAR in the case of band independent uncertainties, $\overline{\upsilon}(N)=0.2$

Spectral bands used				Biome type					
Red	NIR	Blue	Green	Grasses/cereal crops	Shrubs	Broadleaf crops	Savannas	Broadleaf forests	Needle forests
√	√			0.970	0.978	0.897	0.972	0.386	0.666
√	√		√	0.941	0.923	0.843	0.962	0.37	0.573
√			√	0.936	0.909	0.867	0.973	0.719	0.714
√	√	√	√	0.717	0.72	0.685	0.648	0.274	0.395
√		√		0.648	0.697	0.744	0.548	0.634	0.76
√	√	√		0.651	0.708	0.671	0.572	0.267	0.47
		√	√	0.893	0.74	0.808	0.876	0.713	0.513

ophyll abundance and energy absorption. The histograms of NDVI values derived from the SeaWiFS data in July and November 1998 are shown in Fig. 3c and d. Most of the broadleaf and needle forests exhibit very high NDVI values compared to other biomes. On the average, the mean values are 0.67 for broadleaf and 0.71 for needle forests, respectively (Table 1).

It is helpful to introduce a data density function that indicates how densely the pixels occupy the spectral space. Each point in the N-dimensional spectral space represents reflectances $\mathbf{d}=(d_1, d_2, \ldots, d_N)$ of a pixel at N spectral bands. The data density function is defined as the number of points per unit volume about the point **d**. Figs. 3a,b and 4 demonstrate 25% data density contours in different two-

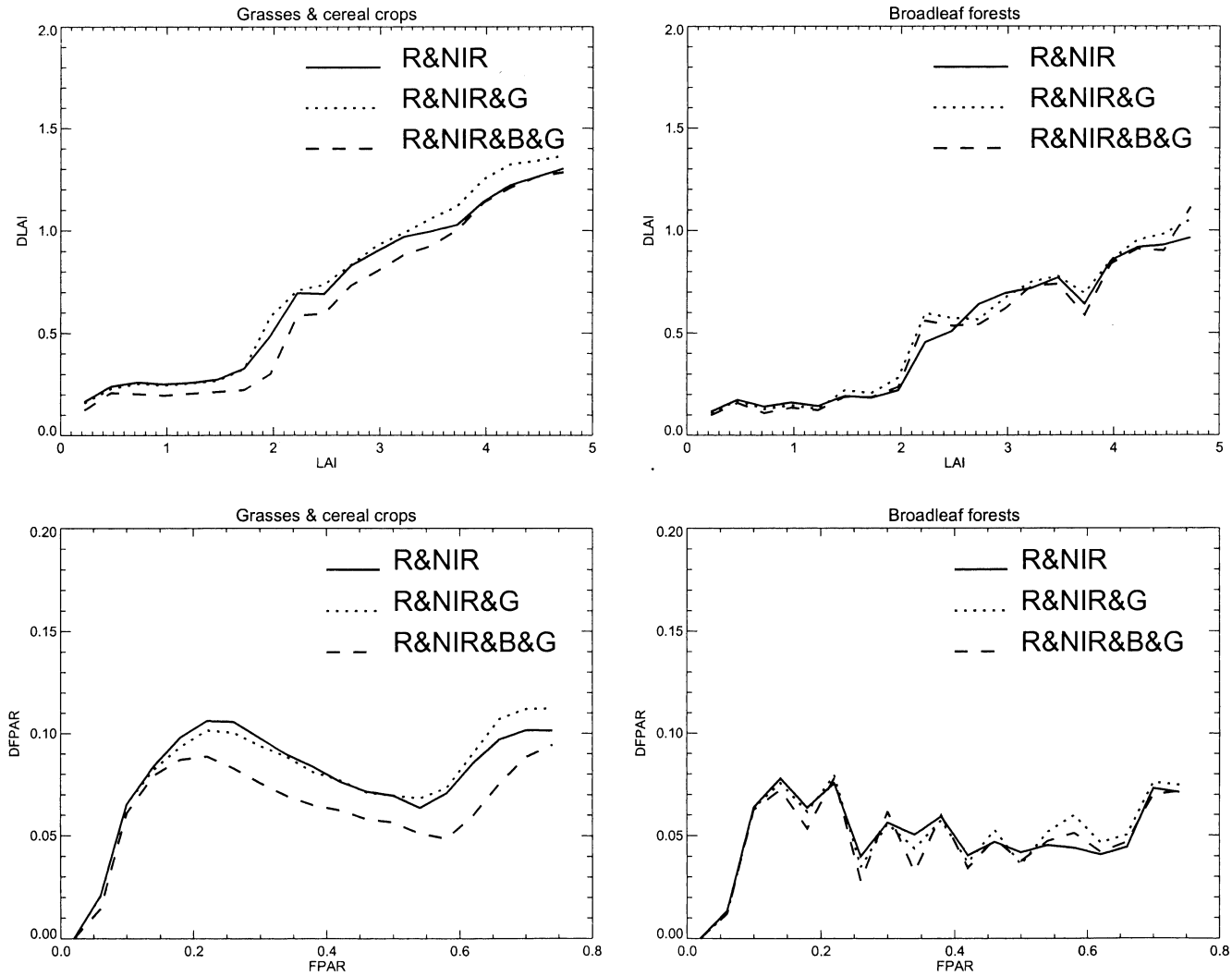

Fig. 6. Dispersions DLAI and DFPAR of retrieved LAI and FPAR values for two biome types (grasses and cereal crops; broadleaf forests) and spectral bands used by the algorithm. The meaning of the labels R&NIR, R&NIR&G, and R&NIR&B&G is the same as in Fig. 5. Relative uncertainties were set to the upper bound 0.2.

Table 4
SI for various combinations of spectral bands used to retrieve LAI and FPAR in the case of band independent uncertainties, $\overline{\upsilon}(N) = 0.2$

Spectral bands used				Biome type					
Red	NIR	Blue	Green	Grasses/cereal crops, %	Shrubs, %	Broadleaf crops, %	Savannas, %	Broadleaf forests, %	Needle forests, %
√	√			13.0	5.8	16.9	10.3	62.2	49.5
√	√		√	13.0	3.7	11.3	10.6	60.3	44.7
√	√	√	√	12.2	3.9	10.6	11.4	60.5	43.3

dimensional spectral spaces. Each contour separates an area on the spectral plane of high data density containing 25% of the pixels from a given biome type. These contours show the most probable location of pixels belonging to a given biome type in the spectral space. The better these contours are separated, the more distinguishable the corresponding biomes are. In the red–NIR plane (Fig. 3a and b) grasses and crops are well separated from forests. In-between these are broadleaf crops and savannas. Both biomes have high NDVI and their contours are close to the NIR axis. The NDVI of grasses and cereal crops is substantially lower and their contours are close to the soil line. Fig. 4 shows that contours can overlap, especially in the red–blue plane. The degree of overlap depends on the resolution of the data (Tian et al., 2000). The contours are maximally separated in the red–NIR plane. This indicates that these two bands

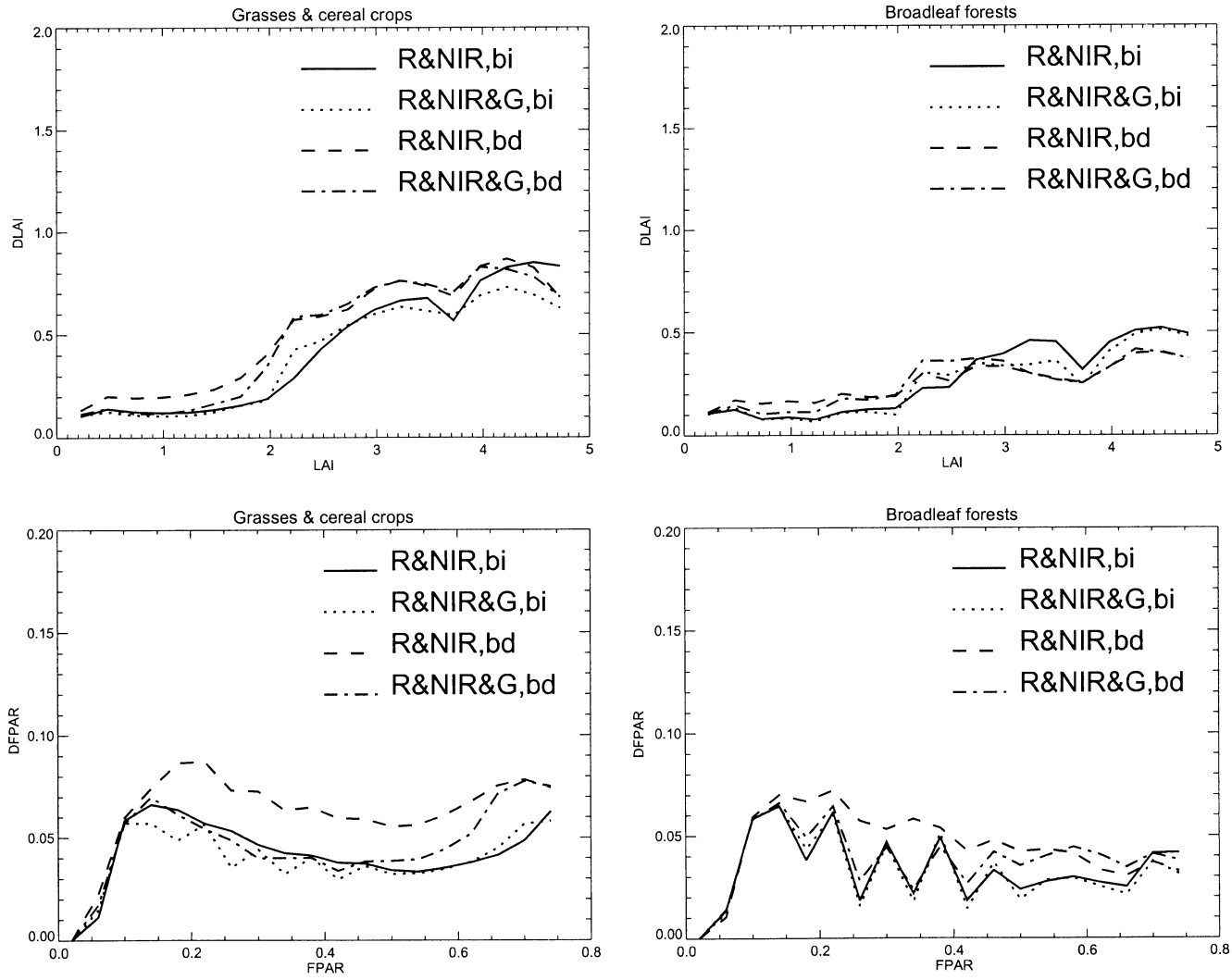

Fig. 7. Dispersions DLAI and DFPAR of retrieved LAI and FPAR values for two biome types (grasses and cereal crops; broadleaf forests) derived from SeaWiFS surface reflectances at red and NIR (label R&NIR); red, NIR and green (label R&NIR&G) spectral bands. Abbreviators "bd" (band dependent) and "bi" (band independent) identify two cases, namely, "bd:" the relative uncertainties depend on wavelength whose values are presented in Table 2; "bi:" the relative uncertainties are wavelength independent, each being set to 0.1.

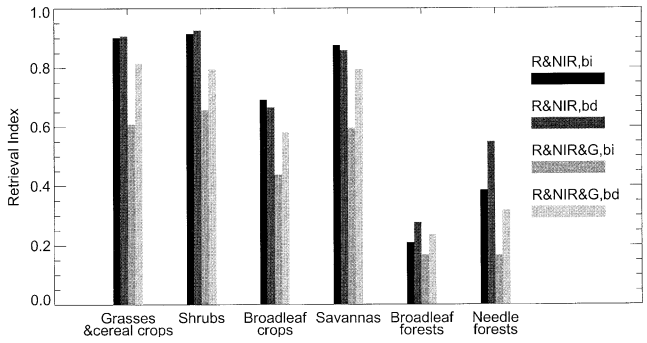

Fig. 8. RI for various biome types and spectral bands used to produce LAIs. Labels have the same meaning as in Fig. 7.

contain maximum information about the biome type, at least, in the case of the 8-km resolution data. This may explain why the algorithm produces reasonable results when using red and NIR data only.

Fig. 3 demonstrates seasonal variation in the contour location and NDVI histogram. All contours move toward the soil line from July (Fig. 3a) to November (Fig. 3b) because of a decrease in LAI. This shift is more pronounced in the case of shrubs. The area of the contours becomes larger in November, which implies a lower data density. The NDVI distributions also show a sharp seasonal change (Fig. 3c and d).

5. Quality of LAI/FPAR retrievals

Monthly minimum-blue composite SeaWiFS reflectances over the vegetated areas in July and November 1998 were chosen as input to the algorithm in this section. The term vegetated pixel is used to refer to pixels of NDVI value greater than 0.1. The algorithm was run pixelwise over all vegetated pixels. In this section, we discuss performance of the algorithm as a function of the number of spectral bands and overall uncertainties.

The relative uncertainties (Eq. (4)) are input to the LAI/FPAR algorithm. However, the SeaWiFS processing does not provide this information routinely. Therefore, we start with the estimation of a possible upper boundary of the overall uncertainty $\overline{\upsilon}(N)$ as follows. Assuming that the relative uncertainties in red, υ_R, and NIR, υ_{NIR}, reflectances are wavelength independent, i.e., $\upsilon_R = \upsilon_{NIR} = \overline{\upsilon}(2)$, find such $\bar{\upsilon}(2)$for which 95% of all land pixels for which Eq. (1) has no solutions for nonvegetated areas and corrupted data due to clouds or atmospheric effect. SeaWiFS surface reflectances at red and NIR spectral bands ($N=2$) acquired over land on September 22 were used to specify $\overline{\upsilon}(2)$. The solution to this problem was $\overline{\upsilon}(2)=0.2$ (Kimes et al., 2000; Knyazikhin, Zhang, Yian, Shabanov, & Myneni, 1998). This value was assigned to $\overline{\upsilon}(N)$. Thus, this upper level of the overall uncertainty allows the algorithm to discriminate between vegetation and nonvegetation reflectances.

The uncertainties in the land surface reflectance product can be estimated from the atmospheric correction algorithm (Kaufman et al., 1997; Vermote et al., 1997). Table 2 shows a theoretical estimate of the relative uncertainties in the MODIS surface reflectance product (Vermote, 2000). The following values were assigned to the relative uncertainties (Eq. (4)) in our study, $\upsilon_R=0.2$ (red), $\upsilon_{NIR}=0.05$ (NIR), $\upsilon_B=0.8$ (blue), and $\upsilon_G=0.1$ (green). The overall relative uncertainty $\overline{\upsilon}(4)$ of the four spectral bands is 0.168, which is quite close to the upper boundary of the overall uncertainty specified above.

To investigate the quality of the LAI/FPAR fields retrieved from multispectral surface reflectances (multiband retrieval), we ran the algorithm using the composite SeaWiFs surface reflectances with: (1) two (red and NIR); (2) three (red, NIR and green); and (3) four (red, NIR, green, and blue) spectral bands as input. The objective of this section was to analyze the use of different combinations of spectral bands to produce LAI and FPAR fields. Special emphasis was given to assessing the influence of relative uncertainties on the quality of the retrieved LAI/FPAR product.

5.1. Multiband retrieval with band-independent uncertainties

It is assumed in this subsection that the relative uncertainties (Eq. (4)) do not depend on wavelength, i.e., $\upsilon_R=\upsilon_{NIR}=\upsilon_B=\upsilon_G$, each being set to upper level of the overall uncertainty 0.2. Fig. 5 shows the RI for various biome types and the number of the input spectral bands used. For a certain uncertainty setting, the RI is a decreasing function of the number of bands. One can see a sharp jump caused by inclusion of the blue surface reflectance in Eq. (1). Table 3 summarizes the use of different combinations of spectral bands in the retrieval technique. All combinations of spectral bands excluding the blue, on the average, have higher values of RI. The following arguments can be presented. The foliage optical properties at

Table 5
SI for various combinations of spectral bands used to retrieve LAI and FPAR in the case of band dependent uncertainties determined in Table 2

Spectral bands used					Biome type					
Red	NIR	Blue	Green	Uncertainty, $\overline{\upsilon}(N)$	Grasses/cereal crops, %	Shrubs, %	Broadleaf crops, %	Savannas, %	Broadleaf forests, %	Needle forests, %
√	√			0.1	8.6	1.4	15.1	8.4	48.8	21.4
√	√		√	0.1	6.5	0.2	6.2	8.9	44.1	9.55
√	√	√	√	0.168	6.3	0.2	5.5	8.0	43.8	10.2

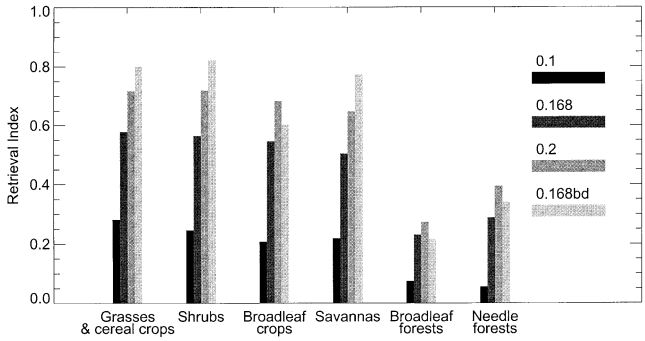

Fig. 9. RI for various biome types and relative uncertainties derived from SeaWiFS surface reflectances at red, near-infrared, green, and blue spectral bands. The bars labeled "0.1," "0.168," and "0.2" correspond to the cases when relative uncertainties in spectral reflectances were wavelength independent and set to 0.1, 0.168, and 0.2, respectively. The label "0.168bd" identifies RIs obtained by using band-specific uncertainties presented in Table 2.

blue and red wavelengths are similar and, thus, the canopy reflectances at these spectral bands are comparable in magnitude. However, atmospheric effect at blue is much stronger than at red and, therefore, uncertainties in the atmospherically corrected surface reflectances are greater at blue than at red band (Table 2). However, these were set to 0.2, i.e., the stabilized uncertainty appears to be substantially underestimated and the RI decreased.

Dispersions of retrieved LAI values for two biome types and various combinations of input spectral bands are shown in Fig. 6. Although some minor differences exist, one cannot see much improvement in the retrieval quality when the number N of bands used to retrieve LAI and FPAR increases. The SI for different combinations of spectral bands is summarized in Table 4. It is only slightly sensitive to N. This implies that we cannot improve accuracy in retrievals by simply including more spectral bands.

5.2. Multiband retrieval with band-dependent uncertainties

Including more spectral information in the retrieval technique initiates two competing processes: increase of information content of data and decrease of overall accuracy in the input data. The first enhances the quality of retrievals, while the second suppresses it. In this subsection, we set values of relative uncertainties to the uncertainties in the land surface reflectance product (Table 2), which are treated as the lower bound of the overall uncertainties. It should be noted that the model uncertainty in canopy reflectance at the green spectral band can be quite high. Indeed, leaf albedo at this wavelength is characterized by temporal variation. For example, a young leaf reflects more energy than an old one. This was not accounted for in our model and, thus, the relative uncertainty at the green wavelength is probably underestimated.

Fig. 7 demonstrates the accuracy of retrieved LAI values derived from surface reflectances at red and NIR wavelengths ($N=2$, legends "R&NIR,bd" and "R&NIR,bi"), and at red, NIR, and green ($N=3$; legends "R&NIR&G,bd" and "R&NIR&G,bi") spectral bands. Abbreviation "bd" (band dependent) and "bi" (band independent) identify two cases. In the first case, the relative uncertainties υ_k depend on wavelength (Table 2). In the second case, relative uncertainties are wavelength independent, each being set to $\bar{\upsilon}(N)=\sqrt[N]{\upsilon_1\upsilon_2\cdots\upsilon_N}$, $N=2$ or 3. Note that in all cases, the overall uncertainty $\bar{\upsilon}(N)$ has the same value (0.1). Again, retrieval dispersions are slightly sensitive to the number N of input spectral bands. However, their values are clearly lower compared to those shown in Fig. 6. This indicates that the retrieval dispersion is sensitive to the overall uncertainty but not to the number N of spectral bands in Eq. (1), i.e., retrieval accuracy is mainly determined by uncertainties in input data. Fig. 8 shows the RI for the four cases described above. The overall uncertainty affects the RI; that is, RI increases with increase of the overall uncertainty

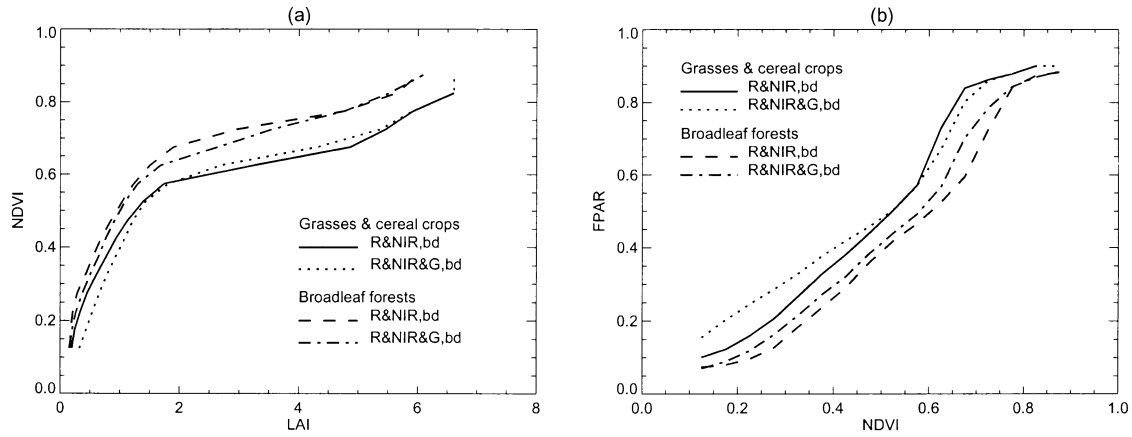

Fig. 10. NDVI/LAI and NDVI/FPAR regression curves for two biome types (grasses and cereal crops; broadleaf forests). LAI and FPAR fields were derived from SeaWiFS surface reflectances at red and near-infrared (label N&NIR) and red, near-infrared and green (label R&NIR&G) spectral bands, which then were regressed against SeaWiFS NDVI. Relative uncertainties listed in Table 2 were used.

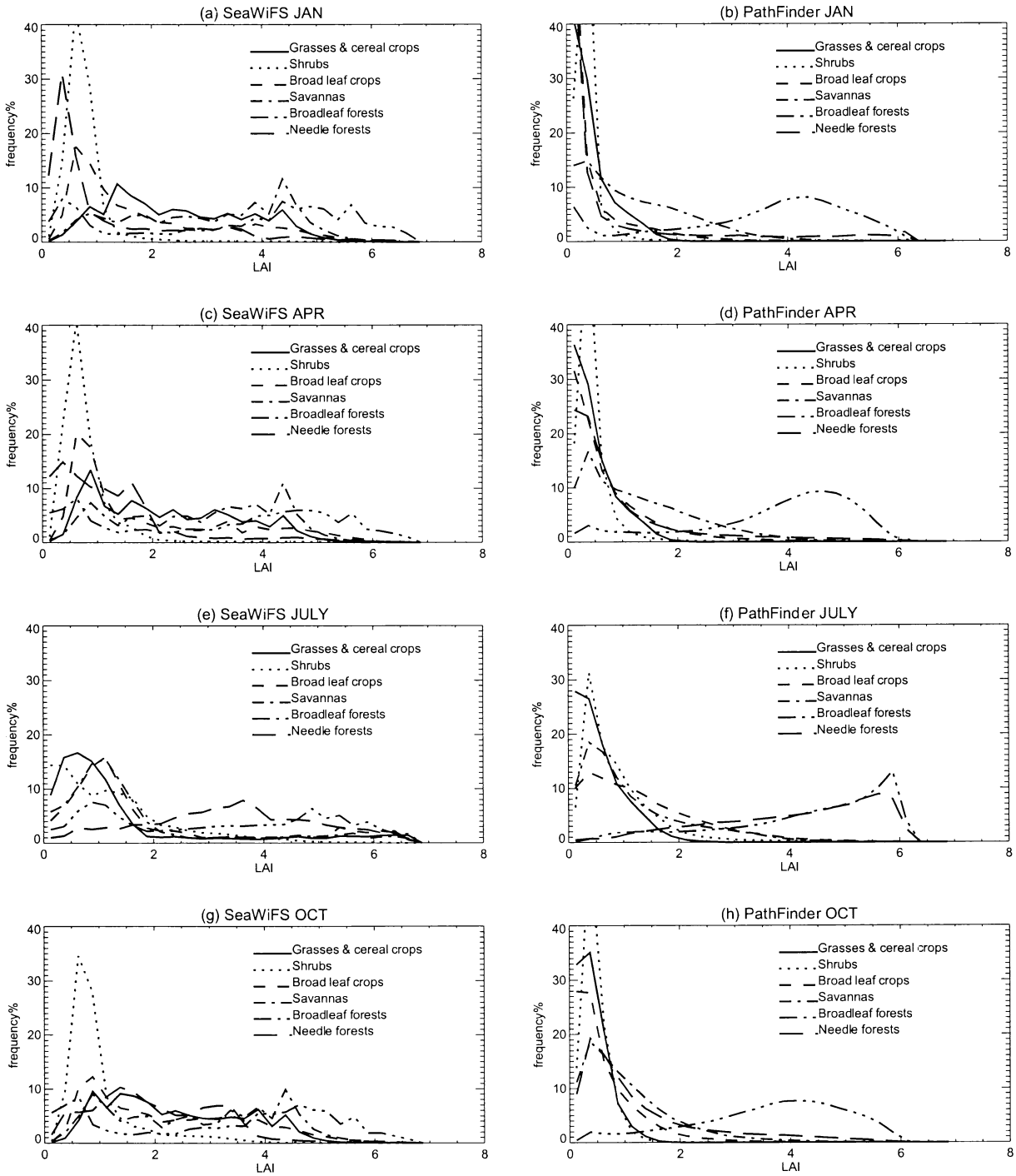

Fig. 11. Seasonal variation of LAI histograms derived from the MODIS LAI/FPAR algorithm with SeaWiFS surface reflectances (right column) and NDVI based algorithm (Myneni et al., 1997) with 10-year averaged Pathfinder data (right column).

(compare Figs. 5 and 8). However, with overall uncertainty constant, an accurate prescription of band-dependent uncertainties results in higher values of the RI (Fig. 8).

Table 5 shows the SI for different biomes and number N ($N=2$, 3, and 4) of input spectral bands. Values of relative uncertainties listed in Table 2 were taken as input for Eqs. (1) and (4). First, the SI decreased compared to those shown in Table 4, i.e., accurate surface reflectance data and models provide higher quality retrievals. Note that the SI is a decreasing function of N (Table 5), and when the overall uncertainty $\overline{\upsilon}(N)$ increases from 0.1 ($N=2$ and 3) to 0.168 ($N=4$), the SI has not increased. Therefore, an increase in the overall uncertainty due to more input spectral bands does not necessarily suppress the increase in information

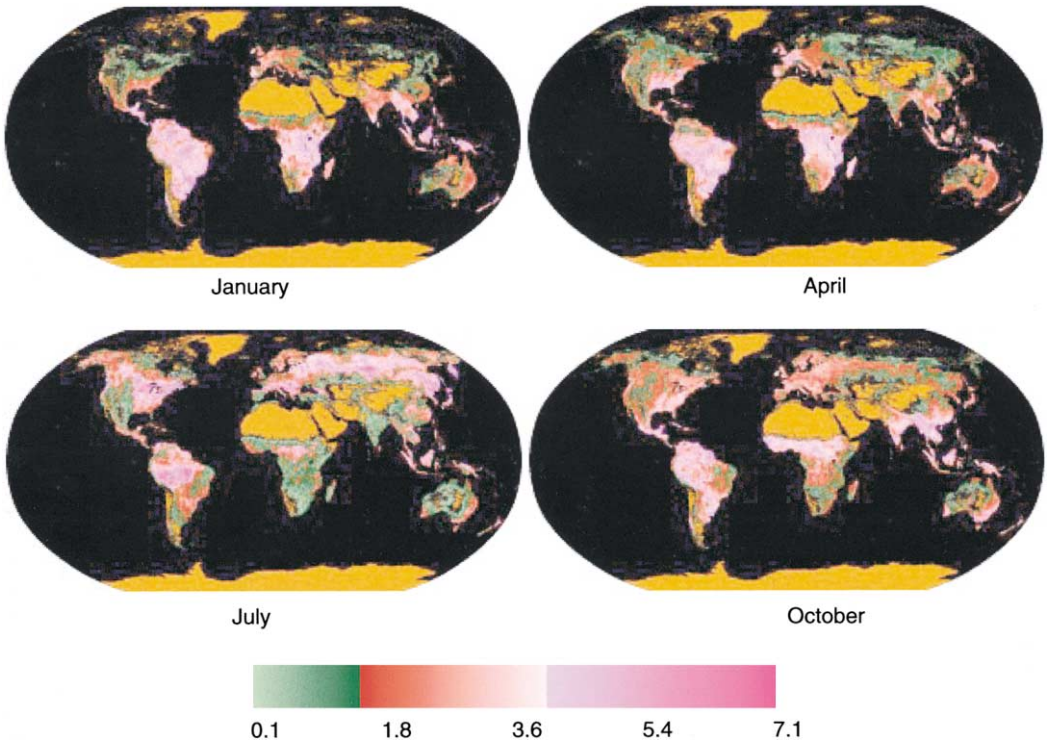

Fig. 12. SeaWiFS global LAI in January, April, July, and October 1998.

supplied to the algorithm if accurate band-specific uncertainties are available.

Fig. 9 demonstrates the RI for $N=4$ (four-band retrieval) as a function of biome type and overall uncertainties. The bars labeled "0.1," "0.168," and "0.2" correspond to the cases when relative uncertainties in spectral reflectances were wavelength independent, i.e. $\nu_k=\overline{\nu}(4)$, and set to 0.1, 0.168, and 0.2, respectively. The legend "0.168bd" identi-

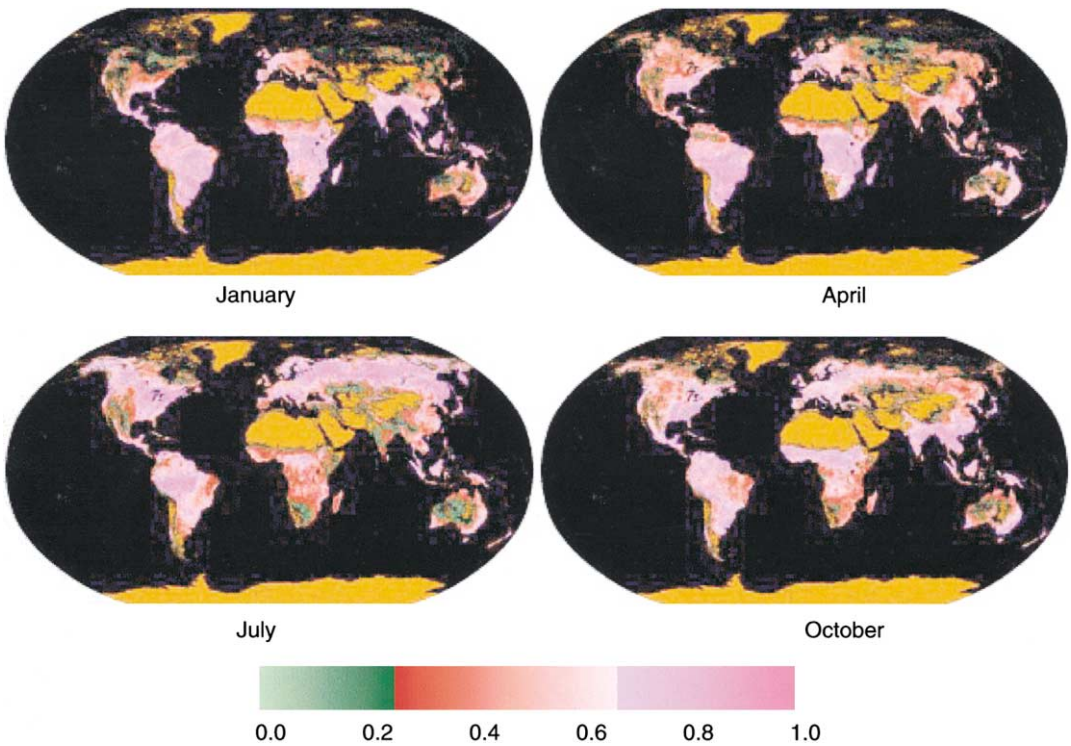

Fig. 13. SeaWiFS global FPAR in January, April, July, and October 1998.

fies retrieval indices obtained by using band-specific uncertainties ν_k (Table 2). One can see that the use of band-specific uncertainties results in higher RI and retrievals of the best possible quality.

5.3. Test of physics

It is well known that there is a strong relationship between a vegetation index, such as NDVI, and surface parameters such as LAI and FPAR (Asrar, Fuchs, Kanemasu, & Harfield, 1984; Chen, 1996; Myneni & Williams, 1994; Peterson, Spanner, Running, & Band, 1987; Tucker & Sellers, 1986; Verma et al. 1993). This relationship provides a method to test the physics of retrievals. Fig. 10 shows the NDVI/LAI and NDVI/FPAR regression curves for two biome types derived using the retrieved LAI and FPAR fields and NDVI computed from SeaWiFS surface reflectances. These correspond to literature reports (Clevers, 1989; Myneni et al., 1997). Note that the LAI values were retrieved directly from surface spectral reflectances without using the NDVI. The advantages of using spectral reflectance rather than NDVI are: (a) NDVI/LAI relations are sensitive to changes in sun angle, view angle, and background reflectance, while the MODIS algorithm actually exploits these changes to retrieve LAI; (b) the NDVI based algorithm can use two spectral bands only, while Eq. (1) can ingest all the available spectral information to improve quality of the retrievals. It should be noted that the retrieved LAI and FPAR fields regressed against SeaWiFS NDVI shown in Fig. 10 were obtained using different combinations of spectral bands as input to Eq. (1). Irrespective of the number of input bands, the NDVI/LAI and NDVI/FPAR relations appear to be close to each other within an accuracy determined by the overall uncertainty $\overline{\upsilon}(N)$. This illustrates algorithm consistence with respect to the physical processes responsible for the observed variation in canopy spectral reflectances.

6. SeaWIFS LAI/FPAR global product

With the above results as guiding principles, we now discuss global LAI/FPAR fields derived from monthly SeaWiFS data from January, April, July, and October. Surface reflectances at red, NIR, and green bands and band-dependent uncertainties listed in Table 2 were used to produce these fields. When the algorithm failed to retrieve a LAI value, the NDVI/LAI and NDVI/FPAR regression curves shown in Fig. 10 were used to estimate LAI and FPAR values. This is similar to the processing for MODIS data.

Histograms of LAI values for the 4 months are shown in Fig. 11. For comparison, a 10-year average global LAI distributions derived from the AVHRR pathfinder 8-km data using a NDVI-based algorithm (Myneni et al., 1997) is also shown in Fig. 11. The histograms clearly show the seasonal variations. Shrubs and needle forests located in the northern hemisphere have low LAI values in the winter (Fig. 11a). During the boreal summer, their LAI increases (Fig. 11e). Savannas in the southern hemisphere have minimum LAI values in the dry period during July (Fig. 11e). Broadleaf forests, which are located in both the northern and southern hemispheres, have a bimodal distribution of LAI.

Figs. 12 and 13 are color-coded images of SeaWiFS LAI and FPAR fields for the 4 months in 1998. In the northern hemisphere, LAI increases from January to a maximum in July and then decreases towards October. On the contrary, because January and April are wet and July is dry season in Africa, LAI values have the lowest values in July. This is consistent with Fig. 11.

7. Conclusions

In this paper, we examine the quality of LAI and FPAR fields derived from SeaWIFs multispectral surface reflectances using the MODIS LAI/FPAR algorithm as a function of input and model uncertainties. When the amount of spectral information input to the LAI/FPAR algorithm is increased, not only does this increase the overall information content but also decreases the summary accuracy in data. The former enhances the quality of retrievals, while the latter suppresses it. The total uncertainty sets a limit on the quality of the retrieved fields. Accurate specification of the uncertainties of inputs to the algorithm is critical to the production of global biophysical variables, and to realize the basic principle of any retrieval technique; that is, the more the measured information and the more accurate this information is, the more reliable and accurate the algorithm output will be. This approach was used to produce global SeaWIFs LAI/FPAR fields of the highest possible quality. Comparing with published results shows this approach works reasonably well.

Acknowledgments

This research was carried out jointly by personnel at Boston University and NASA GSFC under contract with the National Aeronautic and Space Administration.

References

Asrar, G., Fuchs, M., Kanemasu, E. T., & Harfield, J. L. (1984). Estimating absorbed photosynthetic radiation and leaf area index from spectral reflectance in wheat. *Agronomy Journal*, *76*, 300–306.

Bronstein, I. N., & Semendyayev, K. A. (1985). *Handbook of mathematics*. Berlin: Springer (973 pp.).

Carlson, T. N., & Ripley, D. A. (1997). On the relation between NDVI, fractional vegetation cover, and leaf area index. *Remote Sensing of Environment*, *62*, 241–252.

Chen, J. M. (1996). Canopy architecture and remote sensing of the fraction of photosynthetically active radiation absorbed by boreal conifer forests. *IEEE Transactions on Geoscience and Remote Sensing*, *34*, 1353–1368.

Clevers, J.G.P.W. (1989). The application of a weighted infrared–red vegetation index for estimating leaf area index by correcting for soil moisture. *Remote Sensing of Environment*, *29*, 25–37.

Deschamps, P. Y., Bréon, F. M., Leroy, M., Podaire, A., Bricaud, A., Buriez, J. C., & Sèze, G. (1994). The POLDER mission: instrument characteristics and scientific objectives. *IEEE Transactions on Geoscience and Remote Sensing*, *GE-32*, 598–615.

Diner, D. J., Asner, G. P., Davies, R., Knyazikhin, Y., Muller, J. P., Nolin, A. W., Pinty, B., Schaaf, C. B., & Stroeve, J. (1999). New directions in Earth observing: scientific application of multi-angle remote sensing. *Bulletin of the American Meteorological Society*, *80*, 2209–2228.

Gobron, N., Pinty, B., & Verstraete, M. M. (1997). Theoretical limits to the estimation of leaf area index on the basis of visible and near-infrared remote sensing data. *IEEE Transactions on Geoscience and Remote Sensing*, *35*, 1438–1445.

Jasinski, M. F. (1996). Estimation of subpixel vegetation density of natural regions using satellite multispectral imagery. *IEEE Transactions on Geoscience and Remote Sensing*, *34*, 804–813.

Justice, O., Vermote, E., Townshed, J. R. G., Defries, R., Roy, D. P., Hall, D. K., Salomonson, V. V., Privette, J. L., Riggs, G., Strahler, A., Lucht, W., Myneni, R. B., Knyazikhin, Y., Running, S. W., Nemani, R. R., Wan, Z., Huete, A. R., Leeuwen, W. V., Wolfe, R. E., Giglio, L., Muller, J., Lewis, P., & Barnsley, M. J. (1998). The moderate resolution imaging spectroradiometer MODIS: land remote sensing for global research. *IEEE Transactions on Geoscience and Remote Sensing*, *4* (36), 1228–1249.

Kaufman, Y. J., Tanre, D., Remer, L., Vermote, E. F., Chu, A., & Holben, B. N. (1997). Operational remote sensing of tropospheric aerosol over the land from EOS-MODIS. *Journal of Geophysical Research*, *102* (14), 170351–170368.

Kimes, D., Knyazikhin, Y., Privette, J., Abuelgasim, A., & Gao, F. (2000). Inversion methods for physically-based models. *Remote Sensing Reviews*, *18*, 381–439.

Knyazikhin, Y., Martonchik, J. V., Diner, D. J., Myneni, R. B., Verstraete, M., Pinty, B., & Gorbon, N. (1998). Estimation of vegetation canopy leaf area index and fraction of absorbed photosynthetically active radiation from atmosphere-corrected MISR data. *Journal of Geophysical Research*, *103*, 32239–32256.

Knyazikhin, Y., Martonchik, J. V., Myneni, R. B., Diner, D. J., & Runing, S. (1998). Synergistic algorithm for estimating vegetation canopy leaf area index and fraction of absorbed photosynthetically active radiation from MODIS and MISR data. *Journal of Geophysical Research*, *103*, 32257–32275.

Knyazikhin, J., Zhang, Y., Yian, Y., Shabanov, N., Myneni, R. (1998). Radiative transfer based synergistic MODIS/MISR algorithm for the estimation of global LAI&FPAR MODIS quarterly report: Jan/01/98–Mar/31/98, NASA, Greenbelt, MD.

Kuusk, A. (1985). The hot-spot effect of a uniform vegetative cover. *Soviet Journal of Remote Sensing*, *3*, 645–658.

Liu, Q., & Huete, A. (1995). A feedback based modification of the NDVI to minimize canopy background and atmospheric noise. *IEEE Transactions on Geoscience and Remote Sensing*, *33*, 457–465.

Martonchik, J. V., Diner, D. J., Kahn, R., Ackerman, T. P., Verstraete, M. M., Pinty, B., & Gorbon, H. R. (1998). Techniques for the retrieval of aerosol properties over land and ocean using multiangle imaging. *IEEE Transactions on Geoscience and Remote Sensing*, *36*, 1212–1227.

Myneni, R. B. (1991). Modeling radiative transfer and photosynthesis in three-dimensional vegetation canopies. *Agricultural and Forest Meteorology*, *55*, 323–344.

Myneni, R. B., Nemani, R. R., & Running, S. W. (1997). Estimation of global leaf area index and absorbed PAR using radiative transfer models. *IEEE Transactions on Geoscience and Remote Sensing*, *35*, 1380–1393.

Myneni, R. B., & Williams, D. L. (1994). On the relationship between FAPAR and NDVI. *Remote Sensing of Environment*, *49*, 200–211.

Peterson, D. L., Spanner, M. A., Running, R. W., & Band, L. (1987). Relationship of thematic mapper simulator data to leaf area index. *Remote Sensing of Environment*, *22*, 323–341.

Price, J. C. (1993). Estimating leaf area index from satellite data. *Remote Sensing of Environment*, *31*, 727–734.

Ross, J., Knyazikhin, Y., Kuusk, A., Marshak, A., & Nilson, T. (1992). *Mathematical modeling of the solar radiation transfer in plant canopies (in Russian, with English abstract)*. St. Peterburg, Russia: Gidrometeoizdat (195 pp.).

Ross, J. K., & Marshak, A. L. (1984). Calculation of the solar radiation reflection from plant cover using the Monte-Carlo method. *Soviet Journal of Remote Sensing*, *5*, 58–67.

Sellers, P. J., Los, S. O., Tucker, C. J., Justice, C. O., Dazlich, D. A., Collatz, G. J., & Randall, D. A. (1996). A revised land surface parameterization SiB2 for atmospheric GCMs: II. The generation of global field fields of terrestrial biophysical parameters from satellite data. *Journal of Climate*, *94* (4), 706–737.

Sellers, P. J., Randall, D. A., Betts, A. K., Hall, F. G., Berry, J. A., Collatz, G. J., Denning, A. S., Mooney, H. A., Nobre, C. A., Sato, N., Field, C. B., & Henderson-sellers, A. (1997). Modeling the exchanges of energy, water, and carbon between continents and the atmosphere. *Science*, *275*, 502–509.

Tian, Y., Zhang, Y., Knyazikhin, Y., Myneni, R. B., Glassy, J. M., Dedieu, D., & Running, S. W. (2000). Prototyping of MODIS LAI and FPAR algorithm with LASUR and LANDSAT data. *IEEE Transactions on Geoscience and Remote Sensing*, *38* (5), 2387–2401.

Tikhonov, A. N., & Arsenin, V. Y. (1986). *Methods for solving III-posed problems (in Russian)*. Moscow: Nauka (288 pp.).

Tucker, C. J., & Sellers, P. J. (1986). Satellite remote sensing of primary production. *International Journal of Remote Sensing*, *7*, 1395–1416.

Verma, S. B., Sellers, P. J., Walthall, C. L., Hall, F. G., Kim, J., & Goetz, S. J. (1993). Photosynthesis and stomatal conductance related to reflectance on the canopy scale. *Remote Sensing of Environment*, *44*, 103–116.

Vermote, E. (2000). Product accuracy/uncertainty: MOD09, surface reflectance; atmospheric correction algorithm product. In: *MODIS data products catalog (EOS AM Platform)*. Available at: http://modarch.gsfc.nasa.gov/MODIS/RESULTS/DATAPROD/.

Vermote, E. F., Ei Saleous, N. Z., Justice, C. O., Kaufman, Y. J., Privette, J., Remer, L., Roger, J. C., & Tanre, D. (1997). Atmospheric correction of visible to middle infrared EOS-MODIS data over land surface, background, operational algorithm and validation. *Journal of Geophysical Research*, *102* (14), 17131–17141.

Verstraete, M. M., Pinty, B., & Dickenson, R. E. (1990). A physical model of the bidirectional reflectance of vegetation canopies: 1. Theory *Journal of Geophysical Research*, *95*, 11765–11775.

Zhang, Y., Tian, Y., Knyazikhin, Y., Martonchick, J. V., Diner, D. J., Leroy, M., & Myneni, R. B. (2000). Prototyping of MISR LAI and FPAR algorithm with POLDER data over Africa. *IEEE Transactions on Geoscience and Remote Sensing*, *38* (5), 2402–2418.